Space–Time Pulsed Eddy Current Array for NDT of Wellbore Casings Based on MIMO Technique

Changzan Liu, *Student Member, IEEE*, Jingxin Dang, *Student Member, IEEE*, Ling Yang, *Student Member, IEEE*, Yan Zhou, *Member, IEEE*, Xi Luo, and Bo Dang, *Member, IEEE*

***Abstract*— In this article, we present a space–time pulsed eddy current (PEC) array for nondestructive testing (NDT) of wellbore casings using a multiple-input multiple-output (MIMO) technique. On the basis of a multilayered cylindrical wellbore model, an MIMO-PEC model is developed according to the phase shift characteristics of the PEC response corresponding to different transmitting–receiving (TR) distances. To achieve a more significant number of TR channels than in a traditional receiving array to reduce the complexity of the TR structure, a space–time transmission scheme is proposed to recover multiple TR channels. Moreover, a specific space–time MIMO array structure is designed to maximize the number of independent TR channels. The effectiveness of the proposed method is verified by applying the proposed MIMO array to a borehole PEC system for NDT of wellbore casings. The simulation and experimental results demonstrate that using the array structure and space–time transmission scheme proposed in this article, an MIMO structure consisting of M transmitters and N receivers can be equivalent to a transceiver system with a single transmitter and $M \times N$ receivers. Thus, MIMO technique can be effectively applied to PEC-NDT systems and drastically reduce the cost and complexity of the PEC system.**

***Index Terms*— Borehole, multiple-input multiple-output (MIMO), nondestructive testing (NDT), pulsed eddy-current (PEC).**

I. Introduction

RECENTLY, with the increasing concern for safety in oil and gas production, the use of eddy current nondestructive testing (NDT) [1] for wellbore casings has undergone considerable investigation. As a general solution, pulsed (transient) eddy current (PEC) techniques [2], [3] are employed for NDT of wellbore casings [4], [5] as they enable rapid and accurate acquisition of low-frequency range data from time decay signals [6], [7]. A borehole PEC system typically uses pulsed or transient signals as the coil excitation [8], [9], and the metal pipe thickness as well as various defects can be determined by the amplitude and phase of the response received by a magnetic sensor, such as a coil sensor [10], hall sensor [11], and magnetic resistance sensor [12].

Unlike in surface PEC applications, the high temperature [13] and tool shell against downhole pressure [14] significantly affect the borehole PEC testing accuracy of metal pipes [15], [16]. To improve the performance of borehole PEC technologies for metal casing or pipe evaluation, a number of studies have been conducted to understand the effect of the probe parameters of a PEC system [17], [18], [19], [20], [21], [22], [23]. The size and shape of the transmitting and receiving (TR) coils have been demonstrated to significantly affect the performance of the PEC system [17], and varying the coil height and width can offer improved sensitivity [18]. In addition, the number of turns of the coil is important in determining the strength of the magnetic field generated by the coil [19]. In [20], the influence of the emission current parameters, including the pulse waveform and width, on the response signal was analyzed to improve the resolution of the defect depth of the PEC system. Furthermore, much research has been conducted on the distance between the transmitting coil and the receiving coil as another important parameter [21], [22], [23], [24], [25]. In PEC testing of a ferromagnetic casing, Sun et al. [21] divided the spatial distribution of the magnetic field emitted by the transmitting coil into three different regions according to the distance from the transmitting coil and analyzed the response of the receiving coil in each region. In addition, it has been found that the response signal varies with the TR distance, which is similar to the phase difference between different array elements in the phased array radar signal caused by the position of the receiving array element [22], [23], [24].

The phase shift characteristics of the TR distance provide a solid foundation for PEC array processing, and numerous promising results have been reported for PEC testing. In [25], based on the discrepancies caused by the receiver's position, dual receivers were set coaxially to the transmitter to obtain differential signals and remove secondary peaks caused by defects passed by the transmitter. A novel pulsed remote field eddy current probe array was also developed for NDT of ferromagnetic tubes in [26]. Using four detector coils with a small inner diameter distributed along the tube wall with equal spacing, the experimental results demonstrated that the array-based pulsed remote field technique exhibited high precision and sensitivity. In [24], a uniform linear multicoil array-based borehole PEC system for NDT of downhole casings was presented, and the signal received by the multicoil

Manuscript received 6 September 2023; revised 21 October 2023; accepted 25 October 2023. Date of publication 8 November 2023; date of current version 21 December 2023. This work was supported in part by the National Natural Science Foundation of China under Grant 51974250 and Grant 61901371; in part by the Youth Science and Technology Nova Project in Shaanxi Province, China, under Grant 2020KJXX-018; and in part by the Youth Scientific Research and Innovation Team Construction Plan Project of Xi'an Shiyou University under Grant 2022QNKYCXTD02. The Associate Editor coordinating the review process was Dr. Qiang Miao. *(Changzan Liu and Jingxin Dang are co-first authors.) (Corresponding author: Bo Dang.)*

Changzan Liu, Ling Yang, and Bo Dang are with the Shaanxi Key Laboratory of Measurement and Control Technology for Oil and Gas Wells, Xi'an Shiyou University, Xi'an 710065, China (e-mail: bodang521@126.com).

Jingxin Dang is with the School of Resources and Environment, University of Electronic Science and Technology of China, Chengdu 611731, China

Yan Zhou is with the School of Information Science and Technology, Northwest University, Xi'an 710127, China

Xi Luo is with the Well-Tech R & D Institute, China Oilfield Service Limited, Beijing 101149, China

Digital Object Identifier 10.1109/TIM.2023.3331420

array was weighted to cancel the influence of the TR distances of the different array elements and improve the signal-to-noise ratio (SNR) of the system. In [27], [28], and [29], synthesized magnetic field focusing was proposed using a multicoil transmitting array. It was demonstrated that the magnetic field could be synthesized at a particular position by adjusting the current of each transmitting array element, which was calculated according to the distance between each transmitting array element and the magnetic field focusing position. A novel method to calculate the current distribution, which performed magnetic field focusing to improve the receiving SNR, was also proposed in [30] using a multicoil transmitting array. The above studies indicate that signal processing methods using a receiving or transmitting array of sensors are effective in improving detection performance and accuracy.

In recent decades, the improved spatial diversity, parameter identifiability, and detection performance offered by multiple-input multiple-output (MIMO) array systems [31], [32], [33], [34] have led to the widespread use of these systems in a variety of applications, including wireless communication [35], [36], radar and sonar detection [37], [38], [39], and speech recognition [40]. An MIMO array comprises both a transmitter array and a receiver array, where a set of noncoherent orthogonal waveforms are transmitted and can be extracted at the receiver by a corresponding number of matched filters [41]. However, compared to radar systems, the ramp signal used in PEC systems is more difficult to modulate, affecting the application of MIMO technology and the resolution and accuracy of PEC systems. A space–time borehole MIMO-PEC system for NDT of wellbore casings is presented in this article to apply MIMO technology to PEC systems effectively. Based on the borehole PEC signal model, the influence of the number of TR channels with different TR distances on the NDT performance of the PEC array is analyzed. To increase the number of TR channels, a space–time transmission scheme using an MIMO array is proposed. In addition, a space–time multiplexing MIMO array structure is designed to maximize the number of independent TR channels. The simulation and experimental results reveal that the proposed transmission scheme using the designed MIMO array improves the performance of NDT of oil and gas well casing.

The remainder of this article is organized as follows. In Section II, the influence and application of the TR distance based on the borehole PEC signal model are discussed. In Section III, the effect of the number of TR channels is analyzed in the borehole PEC receiving array system. In Section IV, a space–time multiplexing-based transmission scheme based on a borehole MIMO-PEC array is presented, and in Section V, a space–time multiplexing MIMO array structure is designed to maximize the number of independent TR channels. In Section VI, the experimental and simulation results are discussed, and in Section VII, the conclusions are presented.

II. TR Distance Analysis of Borehole PEC System

A borehole PEC system with a multilayer coaxial cylindrical structure is illustrated in Fig. 1. Under the control of the winch, the borehole PEC system is suspended on the cable to realize the NDT of casing pipes. The TR coils have the same inside and outside diameter and are wound around the magnetic core, with their centers located at z_T and z_R on the borehole axis, respectively. According to the multilayer electromagnetic model with coaxial excitation, the induced electromotive force (EMF) of the receiving coil can be obtained as follows [3], [41]:

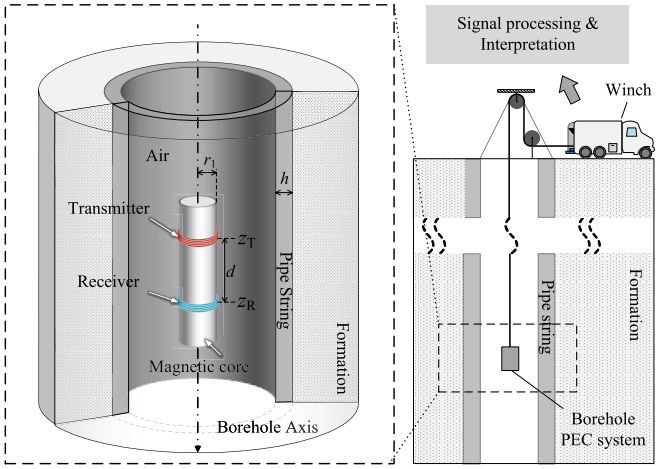

Fig. 1. Borehole pulsed eddy-current system.

$$U(I,d,t,h)=\xi I\int_0^{\infty} f(t,h,\lambda)\cos(\lambda d)d\lambda \tag{1}$$

where I represents the amplitude of the transmitting current, which uses the ramp signal as the pulse (transient) excitation, λ is an introduced variable for solving the Helmholtz equation, and $d = z_T - z_R$ represents the TR distance. In addition

$$f(t,h,\lambda)=\sum_{s=1}^{S} E_s\frac{(e^{-t_{of}s\ln 2/t}-1)}{(s\ln 2/t)}\int_0^{r_1} 2rxCK_0(xr)dr \tag{2}$$

where E_s and S denote the integral coefficient and stage number of the Gaver–Stehfest inverse Laplace transform [3], respectively. t_{of} is the turn-off time, x is an introduced variable satisfying $x^2=\lambda^2-\mu\varepsilon\omega^2+i\mu\sigma\omega$, μ, ε, and σ are the magnetic permeability, capacitance, and conductivity of the core, respectively. $K_0(.)$ represents the modified Bessel function of the second type with order zero. C is the reflection coefficient related to the wall thickness h of the measured casing and the environment under test. Furthermore, $\xi=-\mu N_r N_t r_1/t_{of}$, where N_t and N_r are the numbers of turns of the TR coils, respectively.

In our simulation, assuming that $N_t = 88$, $N_r = 462$, $\mu = 5000$, and $z_T = 0$ mm, the diameter of the core, the outside diameter of the coils, and the inside and outside diameters of the casing were set to 28, 30, 62, and 73 mm, respectively. The winding widths of both the TR coils were 15 mm. We used a ramp signal with a transmitting current of 1 A and a turnoff time of 30 μs as the transient pulse excitation [42] and simulated the induced EMF of the receiving coil at different TR distances by changing the value of z_R (from 10 to 80 mm) based on the finite-element method using COMSOL Multiphysics. The simulation results are presented in Fig. 2(a). It can be seen that the induced EMFs corresponding to different TR distances exhibit the same overall trend of a rapid increase followed by a slow decrease. However, as the TR distance increases, the peak of the induced EMF gradually decreases and appears at a later time. To visualize

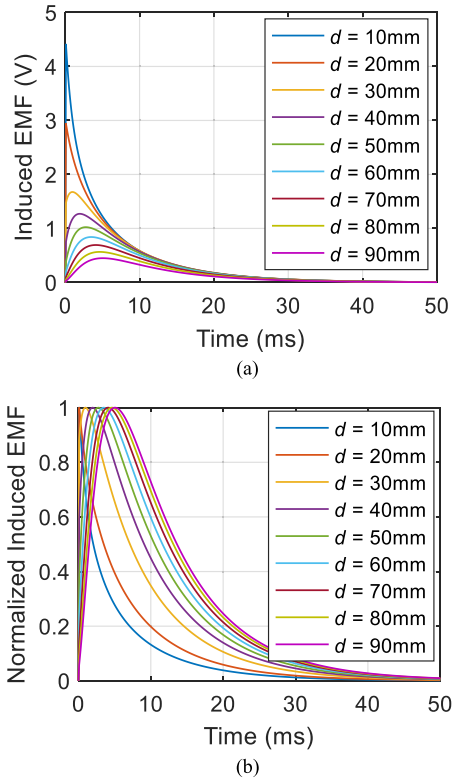

Fig. 2. (a) Induced EMF and (b) normalized induced EMF of the receiving coil with different TR distances.

the difference in the induced EMFs at different TR distances more clearly, we normalized the induced EMFs in Fig. 2(a) and obtained the curves in Fig. 2(b). It can be seen that the normalized induced EMF curves of different TR distances appear indicative of phase shifting similar to that of phased arrays in radar and sonar. To fully utilize multiple configurable receivers to achieve array gain, we revised the borehole PEC received signal model to form an array manifold for further processing.

In this article, the upper limit of integration is approximated as λ_0, and λ is replaced by $\lambda_0(\kappa + 1)/2$. Thus, the induced EMF of the receiving coil can be approximated by converting it into a cumulative sum form using the Gauss–Legendre quadrature rule [43], and the term related to the TR distance is extracted separately [24], [30]. The process can be then expressed as follows:

$$\begin{aligned} &U(I,d,t,h) \\ &\quad\sim \xi I \sum_{p=1}^{P} A_P f\left(t,h,\lambda_0\frac{\kappa_p+1}{2}\right)\cos\left(\lambda_0\frac{\kappa_p+1}{2}d\right) \\ &\quad= \xi I \mathbf{v}^{\mathrm{T}}(d)\mathbf{g}(t,h) \end{aligned} \tag{3}$$

where

$$\begin{aligned} &\mathbf{v}(d) \\ &\quad= \left[\cos\left(\lambda_0\frac{\kappa_1+1}{2}d\right),\ldots,\cos\left(\lambda_0\frac{\kappa_P+1}{2}d\right)\right]^{\mathrm{T}}_{P\times 1} \end{aligned} \tag{4}$$

$$\begin{aligned} &\mathbf{g}(t,h) \\ &\quad= \left[A_1 f\left(t,h,\lambda_0\frac{\kappa_1+1}{2}\right),\ldots,A_P f\left(t,h,\lambda_0\frac{\kappa_P+1}{2}\right)\right]^{\mathrm{T}}_{P\times 1} \end{aligned} \tag{5}$$

where A_p and κ_p are the coefficients and the Gaussian point of the pth-order Gauss–Legendre polynomial, respectively, where P is the number of points of the Gauss–Legendre polynomial [43]. The larger the P is, the closer the value obtained by (3) is to the actual induced EMF. From (3), it can be seen that the target information and casing wall thickness h are included in $\mathbf{G}(t,h)$, and $\mathbf{X}(d)$ can be regarded as the term corresponding to the phase shift generated in Fig. 2(b). Considering the system noise, the induced EMF signal for a receiving array of N elements can be expressed as follows:

$$\begin{aligned} &\mathbf{u}(I,\mathbf{d},t,h) \\ &\quad= \left[U(I,d_1,t,h)\ \ U(I,d_2,t,h)\ \ \cdots\ \ U(I,d_N,t,h)\right]^{\mathrm{T}}_{N\times 1} \\ &\quad= \xi I \mathbf{Y}(\mathbf{d})\mathbf{g}^{\mathrm{T}}(t,h)+\mathbf{n} \end{aligned} \tag{6}$$

where $\mathbf{n}\in\mathbf{R}_{N\times 1}$, and each element of $\mathbf{n}$follows a Gaussian distribution and is independent and identically distributed. $\mathbf{Y}(\mathbf{d})$ denotes the array manifold matrix, and we have

$$\mathbf{Y}(\mathbf{d}) = [\mathbf{v}(d_1),\mathbf{v}(d_2),\ldots,\mathbf{v}(d_N)]^{\mathrm{T}}_{N\times P} \tag{7}$$

where $\mathbf{d} = [d_1,d_2,\ldots,d_N]^{\mathrm{T}}_{N\times 1}$ is a vector consisting of the TR distances of N array elements. The received signals of each element of the receiving array correspond to an independent spatial TR channel with different TR distances. From (6), it can be seen that the same $\mathbf{g}(t,h)$ of each TR channel can be extracted, while the remaining terms of the phase difference are combined into matrix $\mathbf{Y}(\mathbf{d})$. If the weighting matrix $\mathbf{w}\in\mathbf{R}^{N\times 1}$ can be designed such that $\mathbf{w}^{\mathrm{T}}\mathbf{Y}(\mathbf{d}) = \mathbf{f}^{\mathrm{T}}$, where $\mathbf{f}\in\mathbf{R}^{P\times 1}$ is an all-1 row vector representing $\mathbf{v}(0)$ of the channel with a TR distance of 0, the SNR can be improved by fully utilizing multiple TR channels while eliminating the effect of phase difference [28].

According to the linearly constrained minimum variance (LCMV) criterion in array signal processing, we can perform a weighted summation of (6); that is, we can compensate for the phase difference for each received signal before summing [44]. This process is expressed as follows:

$$\begin{aligned} y &= \mathbf{w}^{\mathrm{T}}\mathbf{u}(I,\mathbf{d},t,h) \\ &= \xi I \mathbf{f}^{\mathrm{T}}\mathbf{g}(t,h)+\mathbf{w}^{\mathrm{T}}\mathbf{n}. \end{aligned} \tag{8}$$

The weight vector $\mathbf{w}$ must satisfy the following constraint [44]:

$$\begin{cases} \min \mathbf{w}^{\mathrm{T}}\mathbf{R}_{\mathrm{u}}\mathbf{w} \\ \text{s.t } \mathbf{w}^{\mathrm{T}}\mathbf{V}(\mathbf{d}) = \mathbf{f}^{\mathrm{T}} \end{cases} \tag{9}$$

where $\mathbf{R}_u$ is the autocorrelation matrix of (6). This constraint states that with minimum variance, only the medium- and time-dependent $\mathbf{g}(t,h)$ remains after all TR channels are weighted, and there is no longer a phase difference term. The useful signal is the same except for the noise, which can be summed to achieve coherent accumulation. Moreover, it should be noted that $\mathbf{R}_u$ is related to the sampling time t; therefore, the optimal weights of the signals at different moments in Fig. 2 are different. The constrained problem of (9) can be solved using to the Lagrange multiplier method, and the optimal weight can be expressed as follows [44]:

$$\mathbf{w} = \mathbf{R}_{\mathrm{u}}^{-1}\mathbf{Y}(\mathbf{d})\left(\mathbf{Y}^{\mathrm{T}}(\mathbf{d})\mathbf{R}_{\mathrm{u}}^{-1}\mathbf{Y}(\mathbf{d})\right)^{-1}\mathbf{v}(0). \tag{10}$$

It can be seen that the solution of the weighting coefficients requires the inverse of $\mathbf{Y}^{\mathrm{H}}(\mathbf{d})\mathbf{R}_u^{-1}\mathbf{Y}(\mathbf{d})\in\mathbf{R}^{P\times P}$. And

a necessary and sufficient condition for $\mathbf{Y}^{\mathrm{H}}(\mathbf{d})\mathbf{R}_u^{-1}\mathbf{Y}(\mathbf{d})$ to be reversible is that its rank is equal to P. Since $\mathbf{Y}(\mathbf{d}) \in \mathbf{R}^{N\times P}$ and $\mathbf{R}_u^{-1} \in \mathbf{R}^{N\times N}$, we have

$$\begin{aligned}\operatorname{rank}\left(\mathbf{Y}^{\mathrm{T}}(\mathbf{d})\mathbf{R}_{\mathrm{u}}^{-1}\mathbf{Y}(\mathbf{d})\right) &\le \min\left(\operatorname{rank}\left(\mathbf{R}_{\mathrm{u}}^{-1}\right), \operatorname{rank}(\mathbf{Y}(\mathbf{d}))\right)\\ &\le \min(N, P)\\ &= \begin{cases} P, & N \ge P\\ N, & P > N. \end{cases}\end{aligned} \tag{11}$$

That is, the necessary condition for the weighting coefficients to be solvable is that the number of points P of the Gauss–Legendre polynomial must be less than or equal to the number of TR channels.

From (3), it can be seen that the Gauss–Legendre quadrature results are approximate, and their accuracy can only be improved by increasing the number of points P of the Gauss–Legendre polynomial. Therefore, for the approximation error to be sufficiently small, P is generally chosen to be as large as possible. In the solution of the weighting coefficients of the received signals in the downhole PEC system, when $P < 6$, the solved weighting coefficients are not sufficiently accurate due to the relatively large approximation error of the model, which results in poor performance of the PEC system. Therefore, the number of TR channels affects the accuracy of the weighting coefficients of the received signals, provided that the weighting coefficients can be solved (by ensuring that $\mathbf{Y}^{\mathrm{T}}(\mathbf{d})\mathbf{R}_u^{-1}\mathbf{Y}(\mathbf{d})$ is invertible). The more TR channels there are, the larger P can be set, and the smaller the approximation error of the model will be; thus, the more accurate the weighting coefficients will be. In addition, an increase in the number of TR channels leads to a higher SNR of the PEC system. This phenomenon is similar to that in radar or sonar array signal processing, which can be regarded as array gain.

III. Space–Time PEC Array Using MIMO Technique

Section II demonstrates that an increase in the number of spatial TR channels leads to a higher SNR and reduces the model error. However, in a limited downhole space, a large number of TR channels requires a large number of receivers, which increases the cost and complexity of the PEC system. As a result, it is critical to obtain more channels by using a limited number of array elements. To address this problem, we propose an MIMO-PEC array that allocates a limited number of array elements for TR separately, thereby obtaining more spatial TR channels by using multiple transmitters and receivers.

Suppose that the MIMO-PEC array contains a transmitting array with M elements and a receiving array with N elements, and that both the TR arrays are uniform linear arrays. For the mth transmitter, the induced EMF of the nth receiver at sampling time t is

$$U(I_m, d_{m,n}, t, h) = \xi I_m \mathbf{v}^{\mathrm{T}}\left(d_{m,n}\right)\mathbf{g}(t, x) + N_{m,n}(t) \tag{12}$$

where I_m is the transmitting current of the mth transmitter, $d_{m,n}$ is the TR distance from the mth transmitter to the nth receiver, and noise $N_{m,n}(t)$ follows the same Gaussian distribution as (6). Considering the multiple transmitters and receivers of the MIMO system, spatially, the MIMO-PEC array can form MN spatial TR channels between M transmitters and N receivers. However, since there are only N receivers, the actual received signal is combined as an N-dimensional vector, which is expressed as follows:

$$\begin{aligned}\mathbf{u}_{\mathrm{MIMO}} &= \sum_{m=1}^{M}\left[\, U\left(I_m, d_{m,1}, t, h\right) \quad \cdots \quad U\left(I_m, d_{m,N}, t, h\right)\,\right]^T\\ &= \sum_{m=1}^{M}\left[\, I_m S\left(d_{m,1}, t, h\right) \quad \cdots \quad S\left(d_{m,N}, t, h\right)\,\right]^T\\ &\quad + \sum_{m=1}^{M}\left[\, N_{m,1}(t) \quad \cdots \quad N_{m,N}(t)\,\right]^T\end{aligned} \tag{13}$$

where $S(d_{m,n}, t, h) = \xi \mathbf{v}^{\mathrm{T}}(d_{m,n})\mathbf{g}(t, h)$ denotes the signal part with respect to $(mN + n)$th spatial TR channels. By extracting the transmitting currents to form a vector as $\mathbf{i}_{\mathrm{MIMO}} = [I_1\ I_2, \ldots, I_{\mathrm{M}}]_{1\times M}$, (13) can be rewritten as follows:

$$\mathbf{u}_{\mathrm{MIMO}} = \mathbf{i}_{\mathrm{MIMO}}^{\mathrm{T}}\mathbf{S}(\mathbf{D}, t, x) + \mathbf{n}_{\mathrm{MIMO}}(t) \tag{14}$$

where

$$\mathbf{S}(\mathbf{D}, t, h) = \begin{bmatrix} S\left(d_{1,1}, t, h\right) & \cdots & S\left(d_{1,N}, t, h\right)\\ \vdots & \ddots & \vdots\\ S\left(d_{M,1}, t, h\right) & \cdots & S\left(d_{M,N}, t, h\right)\end{bmatrix}_{M\times N} \tag{15}$$

represents the signal part of MN spatial TR channels, and

$$\mathbf{D} = \begin{bmatrix} d_{1,1} & \cdots & d_{1,N}\\ \vdots & \ddots & \vdots\\ d_{M,1} & \cdots & d_{M,N}\end{bmatrix}_{M\times N} \tag{16}$$

denotes a matrix consisting of MN TR distances. From (14) and (15), it can be seen that although $\mathbf{S}(\mathbf{D}, t, h)$ has a dimension of $M \times N$ that corresponds to the MN spatial TR channels, it is coupled with $\mathbf{i}_{\mathrm{MIMO}}$ to be transformed into a $1 \times N$ vector as a dimensionality reduction operation. As a result, each element of $\mathbf{u}_{\mathrm{MIMO}}$ can be regarded as a summation of the response of a certain receiver to M transmitters, and the actual number of TR channels that can be obtained is only N.

In this article, we propose a space–time transmission scheme to obtain more TR channels of the MIMO-PEC system by recovering MN spatial channels. A diagram of the proposed method is presented in Fig. 3. Similar to the traditional space–time method used in wireless communication and radar systems [35], whose multiple channels are usually recovered at the transmitting end by designing orthogonal waveforms, this study also aims to design a transmitting waveform to recover MN TR channels. However, as illustrated in (14) for the MIMO-PEC system, since the transmitting current $\mathbf{i}_{\mathrm{MIMO}}$ is a row vector of $1 \times M$, it is impossible to recover the information of MN spatial TR channel in $\mathbf{S}(\mathbf{D}, t, h)$ from the coupling of $\mathbf{i}_{\mathrm{MIMO}}$ except for the case of $M = 1$.To solve this problem, we extend a single transmission period to L transmission periods so that the transmitted waveform becomes a matrix with dimensions $M \times L$, comprising M transmitting elements in L transmission periods at the transmitting end.

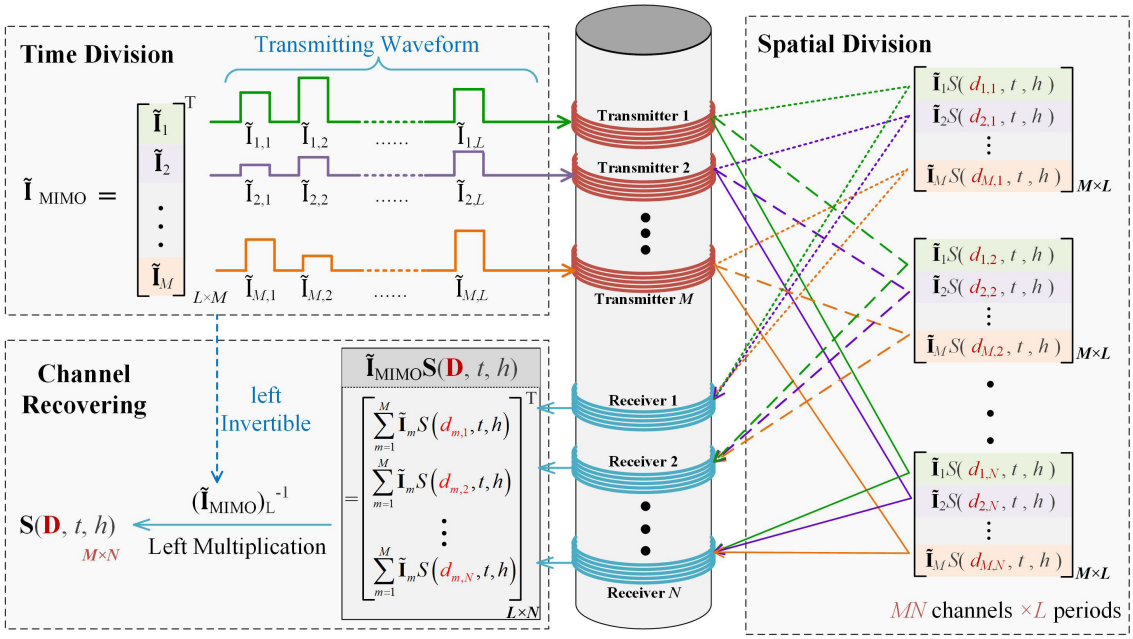

Fig. 3. Proposed space–time transmission scheme using the MIMO pulsed eddy current array.

The waveform matrix composed of the designed transmitting currents is expressed as follows:

$$\tilde{\mathbf{I}}_{\mathrm{MIMO}} = \begin{bmatrix} \tilde{I}_{1,1} & \tilde{I}_{2,1} & \cdots & \tilde{I}_{M,1} \\ \tilde{I}_{1,2} & \tilde{I}_{2,2} & \cdots & \tilde{I}_{M,2} \\ \vdots & \vdots & \ddots & \vdots \\ \tilde{I}_{1,L} & \tilde{I}_{2,L} & \cdots & \tilde{I}_{M,L} \end{bmatrix}_{L\times M} \tag{17}$$

where $\tilde{I}_{m,l}$ denotes the transmitting current of the mth transmitting element in the lth period. Then, the current vector of the mth transmitting element for all L periods can be written as $\tilde{\mathbf{I}}_m = [\tilde{I}_{m,1}\ \tilde{I}_{m,2}, \ldots, \tilde{I}_{m,L}]$. At the receiving end in Fig. 3, the induced EMFs of the nth receiving element in the lth period can be expressed as follows:

$$\tilde{U}_{n,l} = \sum_{m=1}^{M} \tilde{I}_{\mathrm{m},l} S(d_{m,n}, t, h) + \tilde{N}_{n,l}(t) \tag{18}$$

where $\tilde{N}_{n,l}(t)$ is the noise of the nth receiving element in the lth period. The received signals for all N elements with L periods can then be expressed as follows:

$$\begin{aligned} \tilde{\mathbf{U}}_{\mathrm{MIMO}} &= \begin{bmatrix} \tilde{U}_{1,1} & \tilde{U}_{1,2} & \cdots & \tilde{U}_{1,L} \\ \tilde{U}_{2,1} & \tilde{U}_{2,2} & \cdots & \tilde{U}_{2,L} \\ \vdots & \vdots & \ddots & \vdots \\ \tilde{U}_{N,1} & \tilde{U}_{N,2} & \cdots & \tilde{U}_{N,L} \end{bmatrix}^{T}_{L\times N} \\ &= \tilde{\mathbf{I}}_{\mathrm{MIMO}} \mathbf{S}(\mathbf{D}, t, h) + \tilde{\mathbf{N}}_{\mathrm{MIMO}}(t) \end{aligned} \tag{19}$$

where $\tilde{\mathbf{N}}_{\mathrm{MIMO}}(t) \in \mathbf{R}_{L\times N}$ is the noise matrix composed of $\tilde{N}_{n,l}$. Comparing (19) and (13), it can be seen that they both contain the original MN TR channels $\mathbf{S}(\mathbf{D}, t, h)$. However, the coupling matrix is expanded from a $1 \times M$ vector $\mathbf{i}_{\mathrm{MIMO}}$ to an $L \times M$ matrix $\tilde{\mathbf{I}}_{\mathrm{MIMO}}$; therefore, the received signal is also expanded from a $1 \times N$ matrix $\mathbf{u}_{\mathrm{MIMO}}$ to an $L \times N$ matrix $\tilde{\mathbf{U}}_{\mathrm{MIMO}}$ according to the time-division principle.

Therefore, as long as the waveform matrix of the transmitting current $\tilde{\mathbf{I}}_{\mathrm{MIMO}}$ is left-invertible, the $M \times N$ matrix $\mathbf{S}(\mathbf{D}, t, h)$ of the MIMO array can be recovered by left-multiplying $(\tilde{\mathbf{I}}_{\mathrm{MIMO}})_L^{-1}$ to the received signal $\tilde{\mathbf{U}}_{\mathrm{MIMO}}$

$$\begin{aligned} \hat{\mathbf{U}}_{\mathrm{MIMO}} &= \left(\tilde{\mathbf{I}}_{\mathrm{MIMO}}\right)_L^{-1} \tilde{\mathbf{U}}_{\mathrm{MIMO}} \\ &= \left(\tilde{\mathbf{I}}_{\mathrm{MIMO}}\right)_L^{-1} \tilde{\mathbf{I}}_{\mathrm{MIMO}} \mathbf{S}(\mathbf{D}, t, h) + \left(\tilde{\mathbf{I}}_{\mathrm{MIMO}}\right)_L^{-1} \tilde{\mathbf{N}}_{\mathrm{MIMO}}(t) \\ &= \mathbf{S}(\mathbf{D}, t, h) + \left(\tilde{\mathbf{I}}_{\mathrm{MIMO}}\right)_L^{-1} \tilde{\mathbf{N}}_{\mathrm{MIMO}}(t) \end{aligned} \tag{20}$$

where $(\cdot)_L^{-1}$ denotes the left inverse. Furthermore, by reshaping the recovered $\hat{\mathbf{U}}_{\mathrm{MIMO}}$ in (20) from $N \times M$ to $NM \times 1$ according to the TR distances from small to large, the array-weighting algorithm described in Section II can be used to improve the NDT performance. The reshaped $\hat{\mathbf{U}}_{\mathrm{MIMO}}$ can be written as follows:

$$\begin{aligned} \mathbf{u}_{\mathrm{MIMO\text{-}D}} &= \mathrm{vec}\left(\hat{\mathbf{U}}_{\mathrm{MIMO}}\right) \\ &= \chi \mathbf{Y}(\underline{\mathbf{d}}) \mathbf{g}(t, x) + \mathbf{n}_{\mathrm{MIMO\text{-}D}}(t) \end{aligned} \tag{21}$$

where $\underline{\mathbf{d}} = [\underline{d}_1, \underline{d}_2, \ldots, \underline{d}_{MN}]^{\mathrm{T}}_{MN\times 1}$ is the result of sorting the elements of (15) in increasing order. $\mathbf{Y}(\underline{\mathbf{d}}) = [\mathbf{v}(\underline{d}_1), \mathbf{v}(\underline{d}_2), \ldots, \mathbf{v}(\underline{d}_{MN})]^{\mathrm{T}}_{MN\times P}$ is the array manifold matrix of MN channels, and $\mathbf{n}_{\mathrm{MIMO-D}}(t) = \mathrm{vec}[(\tilde{\mathbf{I}}_{\mathrm{MIMO}})_L^{-1} \tilde{\mathbf{N}}_{\mathrm{MIMO}}(t)]_{MN\times 1}$ is the noise vector. From (21), it can be seen that by extending the transmission period of all M transmitting array elements from a single period to L periods, an MIMO array consisting of M transmitters and N receivers can theoretically achieve up to MN channels using the transmitting waveform, which is an $L \times M$-dimensional transmitting current matrix. For comparison, a receiving array consisting of $M + N$ elements can only achieve $M + N - 1$ TR channels. Therefore, by weighting the signal, the space–time MIMO-PEC array proposed in this article can increase the number of TR channels to MN and thereby improve the SNR.

It should be noted that the necessary condition for (20) to recover the signals of MN channels is the existence of the

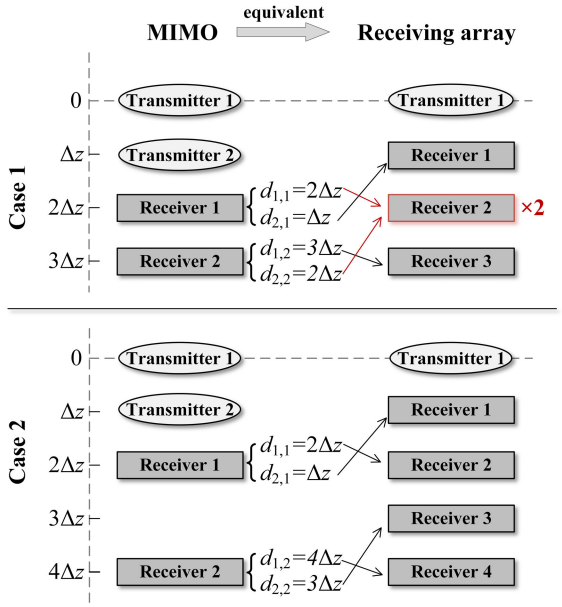

Fig. 4. Two MIMO array layouts and their corresponding receiving array layouts.

left inverse of the transmitting current matrix $\tilde{\mathbf{I}}_{\mathrm{MIMO}}$; that is, $\tilde{\mathbf{I}}_{\mathrm{MIMO}}$ must be full column rank. Therefore, it is necessary to ensure that the number of periods L is greater than or equal to the number of transmitting array elements M, and to design the transmitting current matrix such that $\mathrm{rank}(\tilde{\mathbf{I}}_{\mathrm{MIMO}}) = M$. If L is smaller than M, the left inverse of $\tilde{\mathbf{I}}_{\mathrm{MIMO}}$ does not exist, and the dimensionality of the received induced EMF matrix is too low to recover the signals of MN channels. The most straightforward design scheme is to set $L = M$ and design the transmitting matrix $\tilde{\mathbf{I}}_{\mathrm{MIMO}}$ as an $M \times M$ unit matrix $\mathbf{E}$. However, different transmitting current matrices result in different noise fractions of the final extracted signal, and the design of the transmitting current waveform to achieve improved performance is left for future work.

IV. Space–Time MIMO-PEC Array Design

As illustrated in Section III, it is possible to recover MN TR channels from the MIMO-PEC array to improve the array weighing performance according to the space–time method. However, the full use of MN TR channels requires MN different TR distances. In the receiving array corresponding to the model consisting of a transmitter and multiple receivers, as long as the positions of the receiving array elements are different, the TR distance of each channel is not repeated; that is, the TR channels are independent of each other. In an MIMO-PEC array, this situation is different. From (16), it can be seen that the TR distance of each channel is related to the position of not only the receiving element but also the transmitting element, and the TR distance may be repeated. According to the space–time MIMO-PEC array scheme presented in Section III, we present two cases of different MIMO array distributions consisting of two transmitters and two receivers and their equivalent receiving arrays (illustrated in Fig. 4) as examples.

As illustrated in Fig. 4, the MIMO arrays in both cases can be recovered to four channels with TR distances of $d_{1,1}$, $d_{1,2}$, $d_{2,1}$, and $d_{2,2}$, and each channel is equivalent to the corresponding TR channels in the receiving array according to the TR distance. In Case 1, since $d_{1,1}$ and $d_{2,2}$ are equal and the signal forms of the two TR channels are the same, which are both equivalent to the channel from Transmitter 1 to Receiver 2 in the receiving array. However, in Case 2, the TR distance of each channel is different and is equivalent to four different TR channels of the receiving array. Therefore, $\mathbf{Y}(\underline{\mathbf{d}})$ of (21) in both cases is a $4 \times P$ matrix after channel recovery; however, the row rank of $\mathbf{Y}(\underline{\mathbf{d}})$ in Case 1 becomes 3 after recovery due to the existence of channels with an equal TR distance. According to Section III, to make $\mathbf{Y}^{\mathrm{T}}(\underline{\mathbf{d}})\mathbf{R}_U^{-1}\mathbf{Y}(\underline{\mathbf{d}})$ invertible ($\mathbf{R}_U$ is the autocorrelation matrix of $\mathbf{u}_{\mathrm{MIMO-D}}$), it is necessary to ensure that the number of points of the Gauss–Legendre polynomial is less than the number of independent channels. However, the reduced row rank may lead to an increase in the approximation error.

To avoid repetition of the TR distance, this article also proposes a space–time MIMO-PEC array design method to obtain MIMO arrays with uniform linear arrays at both TR ends. Assuming that the TR distances of MN channels are different and that the equivalent receiving array is an equidistant uniform array with spacing Δz

$$d_{m,n} \in \{\Delta z, 2\Delta z, \ldots, MN\Delta z\}. \tag{22}$$

We also suppose that the position of each TR element can be expressed as follows:

$$\begin{cases} z_{T,m} = (m-1)\Delta z_T + z_{T,1} \\ z_{R,n} = (n-1)\Delta z_R + z_{R,1} \end{cases} \tag{23}$$

where $z_{T,m}$ is the position of the mth transmitting element, $z_{R,n}$ is the position of the nth receiving element, and Δz_T and Δz_R denote the element spacing of the TR arrays of MIMO, respectively. Let all the elements of the transmitting array lie above those of the receiving array; then, the TR distance from the mth transmitting array element to the nth receiving array element can be expressed as follows:

$$\begin{aligned} d_{m,n} &= z_{R,n} - z_{T,m} \\ &= (n-1)\Delta z_R + z_{R,1} - (m-1)\Delta z_T - z_{T,1}. \end{aligned} \tag{24}$$

At this point, the TR distance between the first transmitter and Nth receiver is the largest, while the TR distance between the Mth transmitter and first receiver is the smallest, and we obtain

$$\begin{cases} d_{1,N} = MN\Delta z \\ d_{M,1} = \Delta z. \end{cases} \tag{25}$$

In addition, if the transmitting array element spacing Δz_T is less than the receiving array element spacing Δz_{R}, $d_{M-1,1}$ should be the only TR distance greater than $d_{M,1}$, that is, $d_{M-1,1} = 2\Delta z$. Therefore, the transmitting array element spacing Δz_T is the same as that of the equivalent array of MIMO arrays, that is,

$$\Delta z_T = d_{M-1,1} - d_{M,1} = \Delta z. \tag{26}$$

Letting $z_{T,1} = 0$ and substituting (25) and (26) into (24), we obtain

$$\begin{cases} \Delta z_R = M\Delta z \\ z_{R,1} = M\Delta z. \end{cases} \tag{27}$$

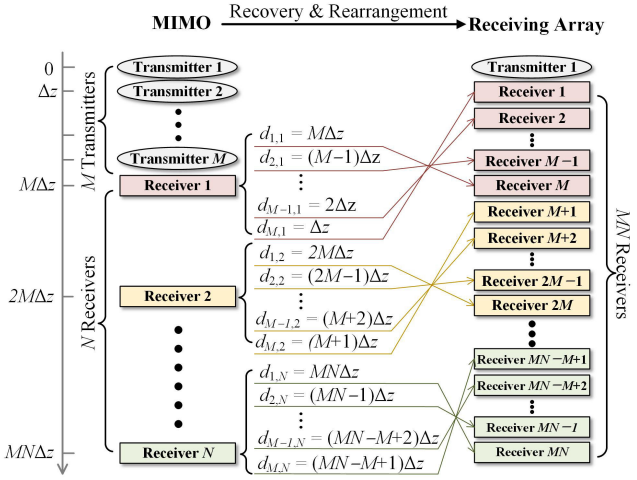

Fig. 5. Distribution of the designed MIMO array and the corresponding receiving array.

Then, we can obtain the position of each array element of the transmitting uniform linear array and the receiving uniform linear array that satisfies (22) as follows:

$$\begin{cases} z_{T,m} = (m-1)\Delta z \\ z_{R,n} = nM\Delta z. \end{cases} \tag{28}$$

Therefore, the TR distance between the mth transmitter and the nth receiver in the MIMO array can be updated as follows:

$$\begin{aligned} d_{m,n} &= z_{R,n} - z_{T,m} \\ &= (nM - m + 1)\Delta z. \end{aligned} \tag{29}$$

According to (28), we can obtain the distribution of the MIMO array designed in this article and the corresponding distribution of the receiving array (presented in Fig. 5).

Fig. 5 indicates that the difference between the TR distance from the mth transmitter to the nth receiver and the TR distance from the kth transmitter to the jth receiver can be expressed as follows:

$$\begin{aligned} d_{m,n} - d_{1,k} &= (nM - m + 1)\Delta z - (kM - j + 1)\Delta z \\ &= ((n-k)M + (j-m))\Delta z. \end{aligned} \tag{30}$$

Since $j - m < M$, (30) can be zero only when $m = j$ and $n = k$, that is, when the TR distances of channels between different transmitters and different receivers are not equal. It can be seen from (29) that the TR distances of MN channels are all multiples of Δz and that the minimum is Δz and the maximum is $MN\Delta z$. Then, the TR distances of all channels of the MIMO array designed according to (28) are $\Delta z, 2\Delta z, \ldots, MN\Delta z$, respectively. Therefore, the MIMO array is equivalent to a uniform receiving array consisting of a single transmitter and MN receivers with element spacing Δz. According to the space–time transmission scheme described in Section III, the signal of each channel can be recovered and recombined as (21). The form of the signal is the same as that of the receiving array consisting of a single transmitter and MN receivers because of the TR distances of MN channels are as follows:

$$\underline{\mathbf{d}} = \begin{bmatrix} \Delta z & 2\Delta z & \cdots & MN\Delta z \end{bmatrix}^T. \tag{31}$$

Therefore, the MIMO-PEC array designed in this article can recover to MN independent channels, which can not only achieve channel multiplication and improve the SNR, but also reduce the approximation error by providing the opportunity to select a larger P. It should be noted that the design method of MIMO array distribution proposed in this article is based on the distance of each channel. Translating the entire designed MIMO array or mirroring and inverting the positions of all array elements centered on any point on the line does not change the TR distance of each channel. In addition, if the functions of the array elements (for TR) are interchanged (i.e., a system consisting of M transmitters and N receivers is converted to a system consisting of M receivers and N transmitters), the TR distance of each channel remains unchanged.

TABLE I
PARAMETERS OF SIMULATION AND FIELD EXPERIMENT

Parameter	Symbol	Value
Radius of transmitters	r_1	28 mm
Inter-element spacing	Δz	20 mm
Number of receiving coil turns	N_R	462
Number of transmitting coil turns	N_T	88
Wire diameter of receiving coils	d_R	0.13 mm
Wire diameter of transmitting coils	d_T	0.33 mm
Length of array	l_A	195 mm
Length of transmitters	l_T	15 mm
Length of receivers	l_R	15 mm

V. EXPERIMENTS AND SIMULATION

The validity of the proposed space–time MIMO-PEC array was evaluated by both simulation and experiments for NDT of wellbore metal casings, where a standard $2^{7/8}$ in casing with a thickness of 5.5 mm and several annular thickness reductions were utilized. To clearly illustrate the effectiveness of the MIMO-PEC array, the results of an MIMO array with three transmitters and three receivers were compared to the results of a traditional receiving array with one transmitter and nine receivers. The number of TR channels for MIMO array and receiving array is equal, and both are 9. The simulation and experiment parameters are presented in Table I, and the structures of the traditional receiving array and the proposed MIMO-PEC array utilized in our simulation and experiment are illustrated in Fig. 6.

As illustrated in Fig. 6, the receiving array has a total of ten elements, including one transmitter and nine receivers, while the proposed MIMO-PEC array has a total of six elements, including three transmitters and three receivers, where the parameters of the transmitters and receivers in the MIMO array and receiving array are the same. Using the space–time transmission scheme, the MIMO-PEC array can achieve nine TR channels like the receiving array by transmitting a set of space–time waveforms and extracting them at the receiver by a corresponding number of matched filters. As described in Section III, the number of periods must be greater than or equal to the number of transmitters to ensure that the transmitting current matrix is left-invertible. Without loss of generality,

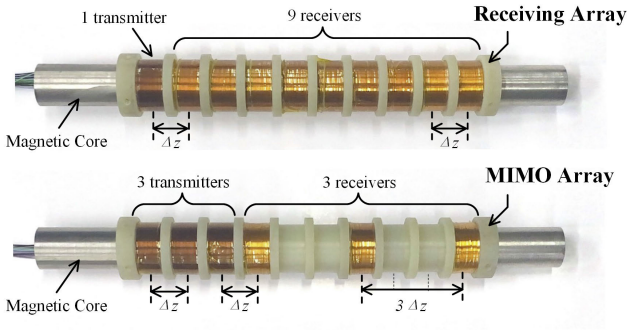

Fig. 6. Proposed MIMO pulsed eddy current array (bottom) and traditional receiving array (top) utilized in the simulation and experiment.

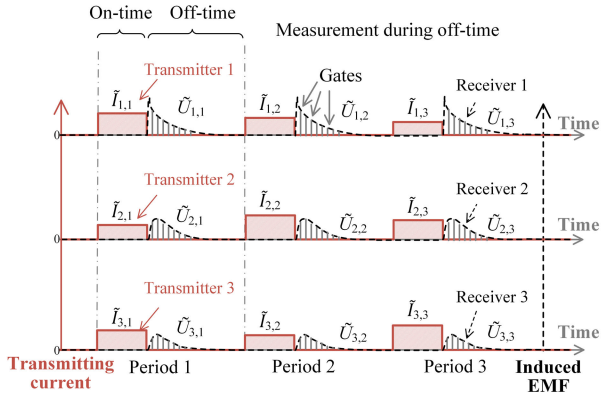

Fig. 7. Diagrammatic sketch of transmitting and Induced EMFs of receivers of space–time MIMO pulsed eddy current array.

we expand each period to three periods, as illustrated in Fig. 7. In each period, the transmitting waveform of each transmitter is a ramp excitation that comprises an on-time part of 100 ms for excitation and an off-time part of 200 ms for measurement. $\tilde{I}_{m,l}$ denotes the transmitting current of the mth transmitter in the lth period mentioned in (17). $\tilde{U}_{n,l}$ represents the induced EMF of the nth receiver in the lth period mentioned in (19), which can be obtained by measurement at different sampling gates.

Notably, the power of each array element is limited by parameters such as the wire diameter in the transmitting system. Therefore, the current values of each transmitter in each period, that is, all elements of $\tilde{\mathbf{I}}_{\mathrm{MIMO}}$, should not exceed the current threshold corresponding to the maximum power of each array element. In this article, the current threshold is assumed to be 1 A. The following is an example of the transmitting current:

$$\tilde{\mathbf{I}}_{\mathrm{MIMO}} = \begin{bmatrix} 1 & 0.8 & 0.6 \\ 0.8 & 1 & 0.8 \\ 0.6 & 0.8 & 1 \end{bmatrix}^{\mathrm{T}}. \tag{32}$$

Using the transmitting waveform in (32), place the PEC array in a standard $2^{7/8}$ in casing with a wall thickness of 5.5 mm, as shown in Fig. 8. At the transmitting end, to avoid mutual electromagnetic interference in the case of individual excitation of each probe, the three transmitting coils are excited simultaneously. At the receiving end, we employ an 8-1 switcher (ADG798) for each receiver to realize the multichannel acquisition, and a high-speed analog-to-digital

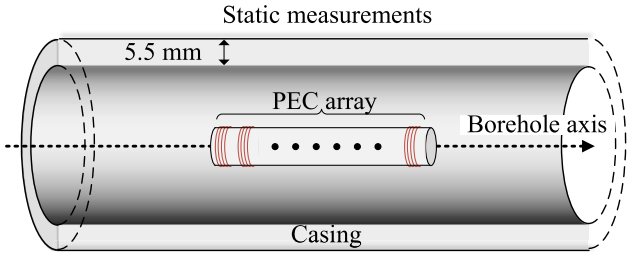

Fig. 8. Experiment structure of the static measurements using PEC array for the NDT of a standard $2^{7/8}$ in casing with a thickness of 5.5 mm.

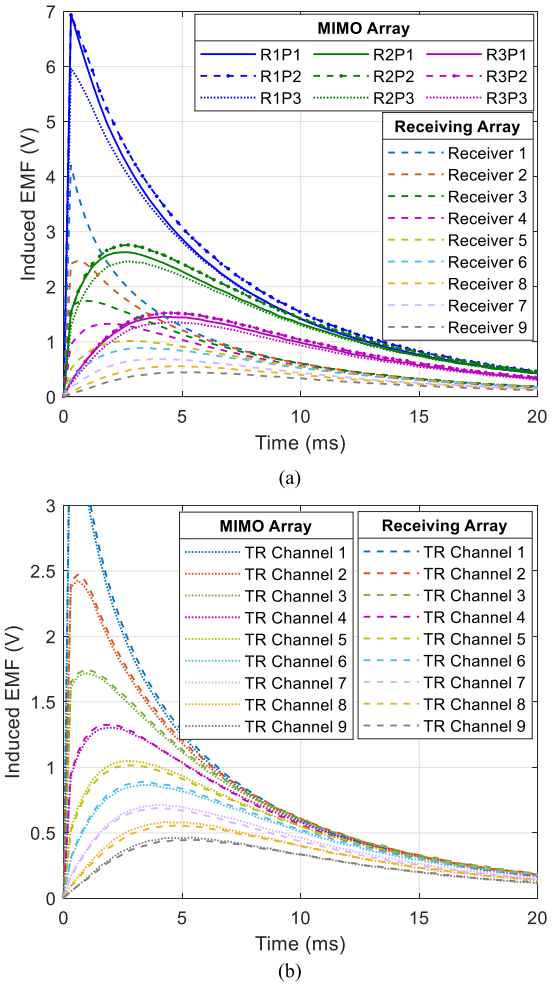

Fig. 9. Comparison of the responses of the receiving array with (a) original responses and (b) recovered nine TR channel data of the MIMO array.

converter (AD7981) is used to sample the PEC responses of different sensors at different sampling times. The original responses and recovered nine TR channel data of the MIMO array and the traditional receiving array are presented in Fig. 9.

Fig. 9(a) presents a comparison of the induced EMFs of the receiving array with those of the three receivers of the MIMO array in three periods, where the induced EMF of the nth receiver in the lth period is referred to as RnPl. The responses of the receiving array represent nine TR channels, which are the same as the nine TR channels of the designed MIMO array. As illustrated in Fig. 9(a), the nine curves for the MIMO array with respect to the three periods and three receivers are different from those of the receiving array with respect to three transmitters and three receivers. Specifically, multiple transmitters of the MIMO array are excited simultaneously in

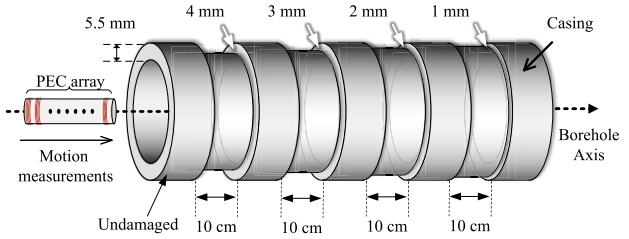

Fig. 10. Experiment structure of the motion measurements with PEC array for the NDT of a standard $2^{7/8}$ in casing with four types of circular symmetry defects.

each period, and the response of the receivers of the MIMO array is the superposition and coupling of the nine TR channels. Fig. 9(b) presents a comparison of the nine TR channels recovered by the nine curves of the MIMO array using the method described in Section III with the nine TR channels of the receiving array. It can be seen that the recovered response curves of the nine TR channels of the MIMO array are highly consistent with the nine response curves of the receiving array, which demonstrates the effectiveness of the space–time transmission scheme and space–time MIMO-PEC array design method.

As described in the analyses in Section III, as long as the space–time transmitting current satisfies the conditions for invertibility, each TR channel can be accurately recovered theoretically. However, the selection of transmitting waveforms affects the power efficiency and the complexity of the recovery process. Considering the implementation complexity, by designing the transmitting current matrix, the transmission weighting and channel recovery can be simplified, and the recovery error can be reduced. For example, using an identity matrix, the TR channels do not need to be recovered with no recovery error. However, an identity matrix of the transmitting current may also result in low-power efficiency. In fact, the power excited by the transmitting array should be adjusted. To maximize the power efficiency, the power of each element of the transmitting array should be maximized. However, a power-maximized transmitting array, such as a transmitting current matrix with all elements of 1, would cause the transmitting current matrix to be invertible. The proposed space–time-based MIMO-PEC array method has a tradeoff design, where a larger number of TR channels are achieved by sacrificing the time and power efficiency. The optimal waveform design of the transmitting array is an interesting direction to pursue to improve the performance of the space–time MIMO array. However, in this article, we focus on the principle and feasibility of the space–time MIMO array, and the design of the transmitting waveform is left for future work.

To further verify the effectiveness of the space–time MIMO array, a set of motion measurements were performed for a section of $2^{7/8}$ in casing (standard thickness of 5.5 mm). In total, four types of circular symmetry defects with thickness reductions of 4, 3, 2, and 1 mm, respectively, were set in an experimental casing as shown in Fig. 10. Furthermore, because the method proposed in this article does not provide a performance advantage in terms of the longitudinal resolution, instead of complex casing structures, a simple set of four defects with a uniform spacing of 10 cm was utilized in the experiments to evaluate the effectiveness of the proposed method for motion measurements. Using the MIMO array in

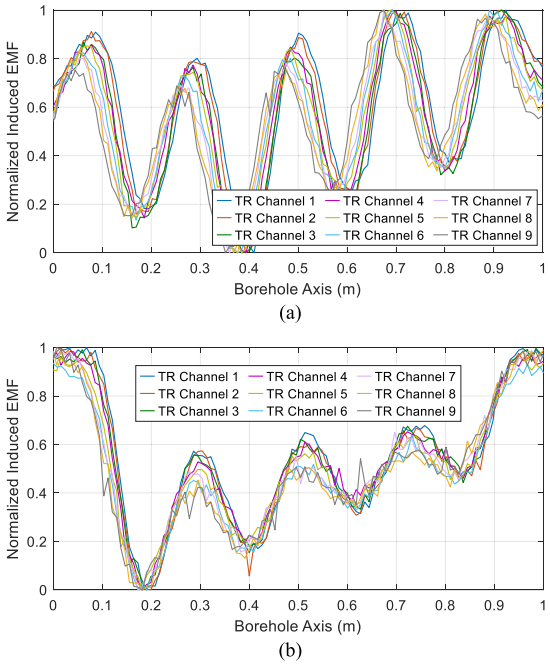

Fig. 11. Nine normalized TR channels of the space–time MIMO pulsed eddy current array at: (a) 5 and (b) 15 ms of motion measurement.

Fig. 6 and the transmitting waveform of (32), the recovered nine TR channels are presented in Fig. 11, where the signals of each TR channel are normalized for clear distinction and comparison.

Fig. 11 presents the nine normalized TR channels of the space–time MIMO-PEC array for NDT of metal casing, where Fig. 11(a) and (b) represents the early stage (5 ms) and late stage (15 ms) of the off-time, respectively. It can be seen that the nine recovered TR channels of the MIMO array are also highly consistent with those of the receiving array in motion measurement for the four different defects in both the early and late stages. In addition, the nine recovered curves corresponding to nine different TR channels can be weighted using the array-weighting method described in Section II, and the weighting results are presented in Fig. 12.

Fig. 12 compares the weighted output curves of the MIMO array, receiving array, and transmitting array with different array element numbers at 5 and 15 ms in three cases. In the first, the weighted output of the designed MIMO array with three transmitters and three receivers (termed MIMO Array—T3R3) is presented, where the total elements number (sums of the number of transmitters and receivers) is 6. For comparison, the weighted output of receiving array [24] with one transmitter and nine receivers (termed receiving array—T1R9) is presented in the second case, where the total element number is 10. In the third case, the weighted output of the transmitting array [30] with nine transmitters and one receiver (termed transmitting array—T9R1) is presented, where the total element number is 10. The three weighting methods used in the comparison adopted different array structures and fit the weighted output of TR channels to the same as the TR channel with the TR distance of 0 to improve the SNR. Although the number of elements in each array structure differs, the TR channel number is all 9 (the number of transmitting elements $\times$ the number of receiving elements). It can be seen

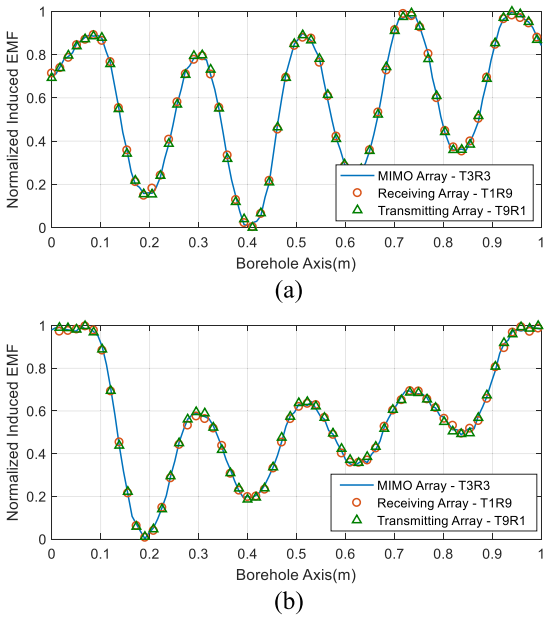

Fig. 12. Comparison of the normalized weighted array output of the MIMO array, receiving array and transmitting array at (a) 5 and (b) 15 ms.

from Fig. 12 that the weighted outputs of the MIMO array, with a lower total number of elements, are highly consistent with those of the receiving array and transmitting array with the same number of TR channels at different sampling times.

In order to quantify the comparison results, the experiment uses a TR channel with the TR distance of 0 as the standard signal and 100 times repeated measurements to obtain a high SNR. Without loss of generality, the root-mean-square error (RMSE) of the weighted output to the standard signal is used to evaluate the performance of the weighting method and is defined as follows:

$$\mathrm{RMSE} = \sqrt{\frac{1}{Q}\sum_{q=1}^{1}\left(Y_q - \bar{U}_q\right)^2} \tag{33}$$

where Y_q and $\bar{U}_q$ denote the weighted output and standard signal of the qth depth, respectively. It should be noted that the RMSE used to evaluate weighting performance is affected by both SNR and weighting error. As demonstrated in Section II, with a larger number of TR channels, a higher SNR can be achieved due to the accumulation of coherent signals. In addition, a larger value of P can be obtained to reduce the model error and improve the accuracy of the weight. Since different total numbers of transmitters and receivers may lead to different numbers of TR channels, the approximation error and weighting performance are also affected. The relationship between the TR channel number, transmitter number, and receiver number is shown in Fig. 13. The experiment and simulation results of the RMSE of different TR channel numbers are presented in Fig. 14.

The number of TR channels that can be achieved is positively correlated with the number of transmitters and receivers and the structure of the array, as shown in Fig. 13. For example, 16 TR channels can be obtained through a receiving array with one transmitter and 16 receivers, a transmitting array with 16 transmitters and one receiver, or an MIMO array with different transmitter and receiver numbers combinations.

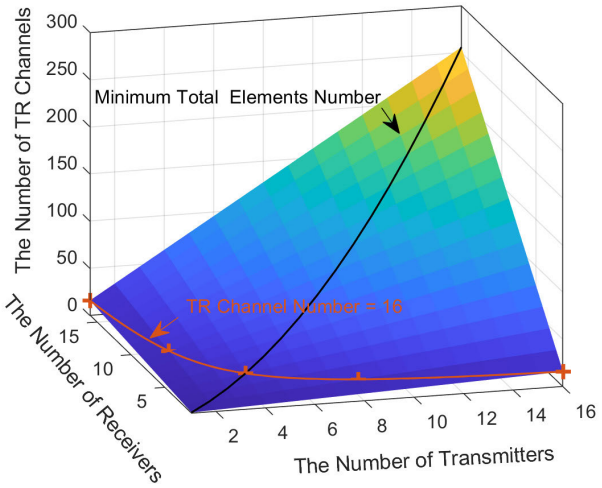

Fig. 13. Relationship between the number of TR channels, the number of transmitters, and the number of receivers.

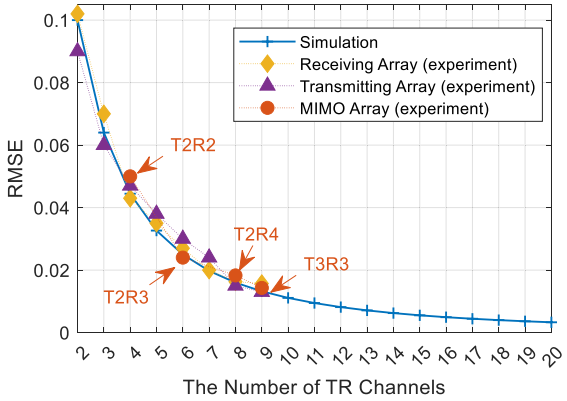

Fig. 14. Experiment and simulation results of the RMSE of different TR channel numbers.

Among them, the MIMO array with four transmitters and four receivers has the lowest total number of elements, and its total number of elements 8 is far less than 17 of the TR arrays. It can be seen from Fig. 13 that the space–time MIMO array can obtain more TR channels than the receiving array with the same total number of array elements due to the multiplication of the number of transmitters of the MIMO array, and the difference becomes greater with the increase in the total number of elements.

Fig. 14 simulates the RMSE as the number of TR channels changes and compares the experimental results with different array structures with different array element numbers. TMRN represents an MIMO array with a transmitter number M and a receiver number N. The simulation results show that RMSE gradually decreases as the number of TR channels increases due to channel gain and the reduction in weighting error caused by multiple TR channels. The experimental results of multiple array structures are consistent with the simulation results, proving this conclusion. In addition, the weighted outputs of the MIMO array are highly consistent with those of the receiving array and transmitting array with the same number of TR channels. Therefore, the MIMO array with only six elements can achieve the same number of TR channels and the same PEC performance as the receiving array or transmitting array with ten elements, which indicates the ability to obtain a large number of TR channels in a borehole

PEC system with a smaller number of array elements and thus reduce the probe complexity.

Moreover, the above experimental and simulation results show that the signal of the separated TR channels MIMO array is very similar to that of the receiving array at different sampling times, and the same processing method can also obtain similar processing results. The comparison and analysis of the output results of the proposed method for the experimental casing structure can also effectively indicate the NDT performance of the proposed method without the need to further explain the thickness. It should be noted that the main contribution of this article is that a small number of array elements can be used to obtain the same multi-TR channel signals as the receiving array for further processing, by using the proposed space–time transmission scheme and designed MIMO-PEC array, which can significantly reduce the complexity and cost of a downhole system in a harsh borehole environment with limited space. In fact, since the separated TR channel signals of MIMO array can be processed in the same way as the signals of the receiving array elements, the array signal processing method and wall thickness interpretation method [45] are not the focus of this article.

VI. Conclusion

In this article, a space–time MIMO-based borehole PEC system is proposed to improve the NDT performance for wellbore casings. On the basis of PEC array signal processing, the influence of the number of independent TR channels is analyzed. The results indicate that an increase in the number of independent channels not only increases the SNR, but also reduces the approximation error. To achieve a larger number of TR channels, an MIMO array with multiple transmitters and receivers is employed, and a space–time transmission scheme is proposed to recover multiple TR channels. Moreover, a space–time MIMO array design method is presented to maximize the number of independent TR channels. Simulation and experimental results on standardized oil well casings show that MIMO arrays with fewer array elements can obtain as many independent TR channels as traditional receiving arrays, thus drastically reducing the complexity of the transceiver module.

References

[1] F. Boßmann, S. Krause-Solberg, J. Maly, and N. Sissouno, "Structural sparsity in multiple measurements," *IEEE Trans. Signal Process.*, vol. 70, pp. 280–291, 2022, doi: 10.1109/TSP.2021.3137599.

[2] T. Meng et al., "Depth evaluation for metal surface defects by eddy current testing using deep residual convolutional neural networks," *IEEE Trans. Instrum. Meas.*, vol. 70, pp. 1–13, 2021, doi: 10.1109/TIM.2021.3117367.

[3] C. Liu et al., "Synthesized magnetic field focusing for the nondestructive testing of oil and gas well casing pipes using pulsed eddy-current array," *IEEE Trans. Magn.*, vol. 58, no. 9, pp. 1–10, Sep. 2022, doi: 10.1109/TMAG.2022.3186548.

[4] H. Malekmohammadi, A. Migali, S. Laureti, and M. Ricci, "A pulsed eddy current testing sensor made of low-cost off-the-shelf components: Overview and application to pseudo-noise excitation," *IEEE Sensors J.*, vol. 21, no. 20, pp. 23578–23587, Oct. 2021, doi: 10.1109/JSEN.2021.3108519.

[5] H. Sun, Y. Shi, W. Zhang, and Y. Li, "Transient eddy current response to pulsed eddy current testing inside a ferromagnetic casing," *NDT & E Int.*, vol. 126, Mar. 2022, Art. no. 102587, doi: 10.1016/j.ndteint.2021.102587.

[6] H. Eskandari and T. Matsuo, "Comparison study of first-order approximations of nonlinear eddy-current field using Cauer ladder network method," *IEEE Trans. Magn.*, vol. 57, no. 6, pp. 1–4, Jun. 2021, doi: 10.1109/TMAG.2021.3060503.

[7] X. Chen and X. Liu, "Pulsed eddy current-based method for electromagnetic parameters of ferromagnetic materials," *IEEE Sensors J.*, vol. 21, no. 5, pp. 6376–6383, Mar. 2021, doi: 10.1109/JSEN.2020.3038203.

[8] B. Yan et al., "Pulse-modulation eddy current imaging for 3D profile reconstruction of subsurface corrosion in metallic structures of aviation," *IEEE Sensors J.*, vol. 21, no. 24, pp. 28087–28096, Dec. 2021, doi: 10.1109/JSEN.2021.3125027.

[9] Z. Yu, F. Yang, Y. Fu, and W. Huang, "Investigation of focusing properties of probes for pulsed eddy current testing," *IEEE Sensors J.*, vol. 21, no. 23, pp. 26830–26838, Dec. 2021, doi: 10.1109/JSEN.2021.3121147.

[10] Q. Xiao, J. Feng, Z. Xu, and H. Zhang, "Receiver signal analysis on geometry and excitation parameters of remote field eddy current probe," *IEEE Trans. Ind. Electron.*, vol. 69, no. 3, pp. 3088–3098, Mar. 2022, doi: 10.1109/TIE.2021.3063958.

[11] E.-H. Toh et al., "A modular three-dimensional hall effect sensor for performance optimization," *IEEE Sensors J.*, vol. 22, no. 12, pp. 11256–11263, Jun. 2022, doi: 10.1109/JSEN.2021.3090211.

[12] Y. Wang, Y. Nie, P. Qi, N. Zhang, and C. Ye, "Inspection of defect under thick insulation based on magnetic imaging with TMR array sensors," *IEEE Trans. Magn.*, vol. 58, no. 3, pp. 1–10, Mar. 2022, doi: 10.1109/TMAG.2021.3138587.

[13] J. M. Salem, F. Lohrabi Pour, and D. S. Ha, "High temperature RF transceiver design for high-speed downhole communications," *Microelectron. J.*, vol. 129, Nov. 2022, Art. no. 105609, doi: 10.1016/j.mejo.2022.105609.

[14] A. Karkevandi-Talkhooncheh, M. Sharifi, and J. Fahimpour, "Estimating reservoir properties using downhole temperature and pressure data," *Geothermics*, vol. 101, May 2022, Art. no. 102359, doi: 10.1016/j.geothermics.2022.102359.

[15] N. Ulapane, K. Thiyagarajan, J. V. Miro, and S. Kodagoda, "Surface representation of pulsed eddy current sensor signals for improved ferromagnetic material thickness quantification," *IEEE Sensors J.*, vol. 21, no. 4, pp. 5413–5422, Feb. 2021, doi: 10.1109/JSEN.2020.3034571.

[16] F. Yuan, Y. Yu, B. Liu, and G. Tian, "Investigation on velocity effect in pulsed eddy current technique for detection cracks in ferromagnetic material," *IEEE Trans. Magn.*, vol. 56, no. 9, pp. 1–8, Sep. 2020, doi: 10.1109/TMAG.2020.3012341.

[17] K. N. Azaman, A. Sophian, and F. Nafiah, "Effects of coil diameter in thickness measurement using pulsed eddy current non-destructive testing," *IOP Conf. Ser., Mater. Sci. Eng.*, vol. 260, Nov. 2017, Art. no. 012001, doi: 10.1088/1757-899x/260/1/012001.

[18] D. Zhou, G. Y. Tian, and Y. Li, "Simulation based on optimisation of pulsed eddy current probe design," *Nondestruct. Test. Eval.*, vol. 25, no. 3, pp. 219–230, Sep. 2010, doi: 10.1080/10589750903242541.

[19] F. Nafiah et al., "Parameter analysis of pulsed eddy current sensor using principal component analysis," *IEEE Sensors J.*, vol. 21, no. 5, pp. 6897–6903, Mar. 2021, doi: 10.1109/JSEN.2020.3036967.

[20] L. Chun-Yu, C. Jin-zhong, S. Guan-nan, and M. Yi-lai, "Design of excitation signal source based on pulsed eddy current technology in pipeline detection system," in *Proc. 7th Int. Symp. Mechatronics Ind. Inform. (ISMII)*, 2021, pp. 65–69, doi: 10.1109/ISMII52409.2021.00021.

[21] H. Sun et al., "A study on ferromagnetic casing wall thinning evaluation based on pulsed eddy current testing," *IEEE Trans. Instrum. Meas.*, vol. 70, pp. 1–11, 2021, doi: 10.1109/TIM.2021.3111002.

[22] S. She, Y. Chen, Y. He, Z. Zhou, and X. Zou, "Optimal design of remote field eddy current testing probe for ferromagnetic pipeline inspection," *Measurement*, vol. 168, Jan. 2021, Art. no. 108306, doi: 10.1016/j.measurement.2020.108306.

[23] H. M. Kim, H. R. Yoo, and G. S. Park, "Analysis of a defect signal deformations induced by eddy current in RFECT system for pipeline inspection," *IEEE Trans. Magn.*, vol. 54, no. 11, pp. 1–5, Nov. 2018, doi: 10.1109/TMAG.2018.2854665.

[24] B. Dang et al., "A uniform linear multi-coil array-based borehole transient electromagnetic system for non-destructive evaluations of downhole casings," *Sensors*, vol. 18, no. 8, p. 2707, Aug. 2018, doi: 10.3390/s18082707.

[25] Q. Luo, Y. Shi, Z. Wang, W. Zhang, and D. Ma, "Method for removing secondary peaks in remote field eddy current testing of pipes," *J. Nondestruct. Eval.*, vol. 36, no. 1, pp. 1–11, Mar. 2017, doi: 10.1007/s10921-016-0379-z.

[26] B. Yang and X. Li, "Pulsed remote eddy current field array technique for nondestructive inspection of ferromagnetic tube," *Nondestruct. Test. Eval.*, vol. 25, no. 1, pp. 3–12, Mar. 2010, doi: 10.1080/10589750802613347.

[27] J. H. Kim, B. H. Choi, H. R. Kim, C. T. Rim, and Y.-S. Kim, "Single-variable-input active sidelobe suppression method for synthesized magnetic field focusing technology and its optimization," *IEEE Trans. Ind. Electron.*, vol. 67, no. 11, pp. 9813–9823, Nov. 2020, doi: 10.1109/TIE.2019.2955408.

[28] Y. Ju, W. Liu, J. Fan, H. Zhou, J. Yu, and X. Zhang, "The optimization simulation of magnetic focus gradient coil for pulsed magnetic field coil," in *Proc. 3rd Int. Conf. Electron. Inf. Technol. Comput. Eng. (EITCE)*, Oct. 2019, pp. 1611–1614, doi: 10.1109/EITCE47263.2019.9095071.

[29] K. Tsukada, T. Hirata, Y. Goda, K. Sakai, and T. Kiwa, "Hybrid magnetic sensor combined with a tunnel magnetoresistive sensor and high-temperature superconducting magnetic-field-focusing plates," *IEEE Trans. Appl. Supercond.*, vol. 29, no. 3, pp. 1–5, Apr. 2019, doi: 10.1109/TASC.2018.2874354.

[30] C. Liu et al., "Multiple-transmit focusing for the nondestructive testing of downhole casings based on borehole transient electromagnetic systems," *IEEE Access*, vol. 8, pp. 210978–210987, 2020, doi: 10.1109/ACCESS.2020.3037944.

[31] Z. Wang, Q. He, and R. S. Blum, "Target detection using quantized cloud MIMO radar measurements," *IEEE Trans. Signal Process.*, vol. 70, pp. 1–16, 2022, doi: 10.1109/TSP.2021.3129364.

[32] E. Shi et al., "Wireless energy transfer in RIS-aided cell-free massive MIMO systems: Opportunities and challenges," *IEEE Commun. Mag.*, vol. 60, no. 3, pp. 26–32, Mar. 2022, doi: 10.1109/MCOM.001.2100671.

[33] P. Sharma, R. N. Tiwari, P. Singh, P. Kumar, and B. K. Kanaujia, "MIMO antennas: Design approaches, techniques and applications," *Sensors*, vol. 22, no. 20, p. 7813, Oct. 2022, doi: 10.3390/s22207813.

[34] Á. A. Pingarrón, "Antarctic ice tomography with airborne MIMO synthetic aperture radar," Univ. College London, London, U.K., Tech. Rep., 2020. [Online]. Available: https://discovery.ucl.ac.uk/id/eprint/10116231

[35] A. Salam and U. Raza, "Spatial modulation: Subsurface MIMO," in *Signals in the Soil Developments in Internet of Underground Things*. Cham, Switzerland: Springer, 2020, pp. 140–147.

[36] J. Zhang, J. Zhang, D. W. K. Ng, S. Jin, and B. Ai, "Improving sum-rate of cell-free massive MIMO with expanded compute-and-forward," *IEEE Trans. Signal Process.*, vol. 70, pp. 202–215, 2022, doi: 10.1109/TSP.2021.3129337.

[37] Z. Xu, C. Fan, and X. Huang, "MIMO radar waveform design for multipath exploitation," *IEEE Trans. Signal Process.*, vol. 69, pp. 5359–5371, 2021, doi: 10.1109/TSP.2021.3112042.

[38] X. Liu, R. Shi, C. Sun, Y. Yang, and J. Zhuo, "Using deconvolution to suppress range sidelobes for MIMO sonar imaging," *Appl. Acoust.*, vol. 186, Jan. 2022, Art. no. 108491, doi: 10.1016/j.apacoust.2021.108491.

[39] H. Yang, T. Li, N. Li, Z. He, and Q. H. Liu, "Efficient near-field imaging for single-borehole radar with widely separated transceivers," *IEEE Trans. Geosci. Remote Sens.*, vol. 53, no. 10, pp. 5327–5337, Oct. 2015, doi: 10.1109/TGRS.2015.2421478.

[40] J. Li, Y. Zhu, D. Luo, Y. Liu, G. Cui, and Z. Li, "The PCG-AIID system for L3DAS22 challenge: MIMO and MISO convolutional recurrent network for multi channel speech enhancement and speech recognition," in *Proc. IEEE Int. Conf. Acoust., Speech Signal Process. (ICASSP)*, May 2022, pp. 9211–9215, doi: 10.1109/ICASSP43922.2022.9746055.

[41] F. Liu, Y.-F. Liu, A. Li, C. Masouros, and Y. C. Eldar, "Cramér–Rao bound optimization for joint radar-communication beamforming," *IEEE Trans. Signal Process.*, vol. 70, pp. 240–253, 2022, doi: 10.1109/TSP.2021.3135692.

[42] A. Dashevsky and A. Yu, *Principles of Induction Logging*. Amsterdam, The Netherlands: Elsevier, 2003.

[43] D. Si, J. Wang, G. Wei, and X. Yan, "Method and experimental study of voltage measurement based on electric field integral with Gauss–Legendre algorithm," *IEEE Trans. Instrum. Meas.*, vol. 69, no. 6, pp. 2771–2778, Jun. 2020, doi: 10.1109/TIM.2019.2924571.

[44] J.-Q. Lin and S.-C. Chan, "Recursive extended instrumental variable based LCMV beamformers for planar radial coprime arrays under spatially colored noise," *IEEE Trans. Aerosp. Electron. Syst.*, vol. 57, no. 1, pp. 175–189, Feb. 2021, doi: 10.1109/TAES.2020.3011870.

[45] D. Wen, M. Fan, B. Cao, B. Ye, and G. Tian, "Lift-off point of intersection in spectral pulsed eddy current signals for thickness measurement," *IEEE Sensors Lett.*, vol. 2, no. 2, pp. 1–4, Jun. 2018, doi: 10.1109/LSENS.2018.2822296.

Changzan Liu (Student Member, IEEE) was born in Hebei, China, in 1989. He received the Ph.D. degree in signal and information processing from Northwestern Polytechnical University, Xi'an, China, in 2022.

Since 2023, he has been taught with the Department of Electronic Engineering, Xi'an Shiyou University, Xi'an. His research interests include downhole pulsed eddy-current system for nondestructive testing and evaluation of casing and tubing.

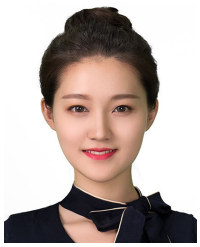

Jingxin Dang (Student Member, IEEE) received the B.S. degree in electrical engineering and automation from Xi'an Polytechnic University, Xi'an, China, in 2018, and the M.S. degree in electronic engineering with management from King's College London, London, U.K., in 2020. She is currently pursuing the Ph.D. degree in information and communication engineering with the University of Electronic Science and Technology of China, Chengdu, China.

Her research interests include signal processing, electromagnetic logging, and electromagnetic imaging.

Ling Yang (Student Member, IEEE) was born in Xi'an, Shaanxi, China, in 1993. She is currently pursuing the Ph.D. degree in oil and gas engineering with Xi'an Shiyou University, Xi'an.

Her research interests include downhole transient electromagnetic oil and gas resource detection.

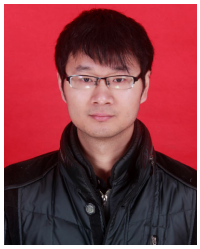

Yan Zhou (Member, IEEE) received the B.E. and Ph.D. degrees from Xidian University, Xi'an, China, in 2010 and 2015, respectively.

He is currently an Associate Professor with the School of Information Science and Technology, Northwest University, Kirkland, WA, USA. His research interests include space–time adaptive processing and array signal processing.

Xi Luo was born in 1980. He received the M.S. degree from the University of Electronic Science and Technology of China, Chengdu, China, in 2006.

He is currently a Senior Engineer and works at the Well-Tech Research and Development Institute, China Oilfield Services Ltd., Beijing, China. He is mainly involved in research on geophysical logging methods.

Bo Dang (Member, IEEE) was born in Xi'an, China, in 1987. He received the B.E. and Ph.D. degrees from Xidian University, Xi'an, in 2008 and 2013, respectively.

He is currently a Professor with the Department of Electronic Engineering, Xi'an Shiyou University, Xi'an. His research interests include downhole transient electromagnetic system for nondestructive testing and evaluation of casing and tubing.